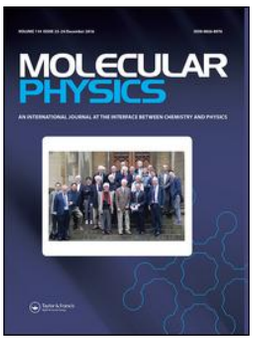

Taylor & Francis
Taylor & Francis Group

Molecular Physics

An International Journal at the Interface Between Chemistry and Physics

ISSN: 0026-8976 (Print) 1362-3028 (Online) Journal homepage: http://www.tandfonline.com/loi/tmph20

Vapour–liquid phase equilibrium and surface tension of fully flexible Lennard–Jones chains

Kevin S. Silmore, Michael P. Howard & Athanassios Z. Panagiotopoulos

To cite this article: Kevin S. Silmore, Michael P. Howard & Athanassios Z. Panagiotopoulos (2017) Vapour–liquid phase equilibrium and surface tension of fully flexible Lennard–Jones chains, Molecular Physics, 115:3, 320-327, DOI: 10.1080/00268976.2016.1262075

To link to this article: http://dx.doi.org/10.1080/00268976.2016.1262075

Published online: 07 Dec 2016.

Submit your article to this journal

Article views: 51

View related articles

View Crossmark data

Full Terms & Conditions of access and use can be found at
http://www.tandfonline.com/action/journalInformation?journalCode=tmph20

Download by: [Princeton University] **Date:** 04 January 2017, At: 10:44

MOLECULAR PHYSICS, 2017
VOL. 115, NO. 3, 320–327
http://dx.doi.org/10.1080/00268976.2016.1262075

Taylor & Francis
Taylor & Francis Group

RESEARCH ARTICLE

Vapour–liquid phase equilibrium and surface tension of fully flexible Lennard–Jones chains

Kevin S. Silmore *, Michael P. Howard * and Athanassios Z. Panagiotopoulos *

Department of Chemical and Biological Engineering, Princeton University, Princeton, NJ, USA

ABSTRACT

We report measurements of the vapour–liquid coexistence densities and surface tension of fully flexible Lennard–Jones chain molecules ranging in length from 4 to 60 beads. We demonstrate that the surface tension for all chain lengths collapses to a single master curve when plotted according to the universal parachor correlation. We find a universal parachor exponent 3.79 ± 0.05 for conditions close to the critical point, with a deviation observed for the longest chains far below the critical point.

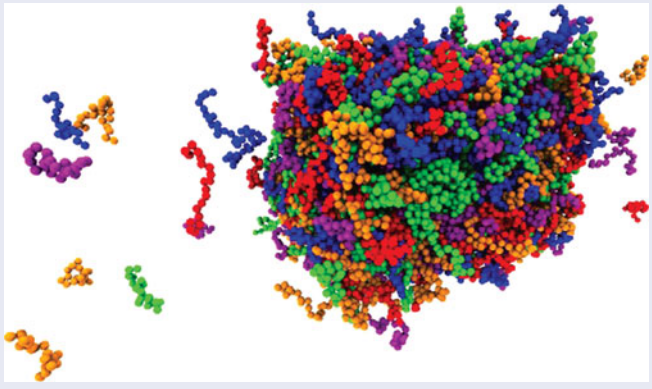

ARTICLE HISTORY
Received 16 September 2016
Accepted 11 November 2016

KEYWORDS
Lennard–Jones chain; surface tension; vapour–liquid; parachor; corresponding states

1. Introduction

The surface tension of high-molecular-weight polymers is a key material property for technological processes such as enhanced oil recovery [1] and the production of organic electronics [2]. Unfortunately, it is challenging to measure the surface tension of chain molecules over large ranges of temperature and molecular weight due to increased melt viscosity at higher molecular weights, thermal instabilities and sample polydispersity [3]. For example, reliable experimental surface tension data for the homologous series of *n*-alkanes only exists for low molecular weights (up to approximately $C_{20}H_{42}$) [4,5] and for commercial polyethylenes [6]. Recently, square gradient theory has been successfully applied to predict the surface tension of the *n*-alkane series and other small-molecule industrial fluids [7]. In cases where theoretical predictions are difficult to obtain, reasonable estimates of the surface tension can instead be made from correlations based on measurable thermodynamic properties. It remains an important challenge to validate general correlations for the surface tension of long chain molecules.

The parachor correlation, introduced empirically by Macleod [8] and extended by Sugden [9], relates the surface tension γ to the coexistence densities:

$$\gamma = \left(\frac{P \Delta \rho}{M} \right)^p ,$$

where P is the material-specific parachor, $\Delta\rho = \rho_L - \rho_V$ is the difference in liquid and vapour densities, M is the molecular weight and p is the universal parachor exponent, originally proposed to be equal to 4. Guggenheim [10] applied the principle of corresponding states and found that $p = 11/3$. Considerations of universal critical phenomena for γ and $\Delta\rho$ suggest that $p = 3.87$ near the critical point [11]. In practice, fitted values for p

CONTACT Athanassios Z. Panagiotopoulos azp@princeton.edu
*These authors contributed equally to this work.

© 2016 Informa UK Limited, trading as Taylor & Francis Group

generally range from 3.5 to slightly larger than 4. Although useful as an engineering correlation, the parachor approach has limited transferability for different materials due to the need to determine or estimate P.

More recently, the 'universal parachor' approach [12,13], which combines the parachor with the principle of corresponding states, has been proposed to correlate surface tension with the coexistence densities and critical properties. The reduced surface tension,

$$\gamma^* = \frac{\gamma}{k_B T_c (\rho_c/M)^{2/3}},$$

appears to be a universal function of $\Delta\rho/\rho_c$ for molecules of various geometries excluding those that exhibit hydrogen bonding, such as water [13]. Here, k_B is Boltzmann's constant, T_c is the critical temperature and ρ_c is the critical density. In particular, a power-law relation

$$\gamma^* \sim (\Delta\rho/\rho_c)^p, \tag{1}$$

with an exponent $p = 3.55$ has been shown to describe the data well [12,13]. Molecular simulations have been used to validate the universal parachor relation for a variety of model oligomers, such as the fully flexible Lennard–Jones chain [14], up to 16 beads in length [15]. It remains untested whether the universal parachor relation applies to longer chain molecules.

Despite recent renewed interest in the interfacial properties of Lennard–Jones chains [16–20], only sparse data exists for chains longer than 16 beads [14,21,22]. In this article, we report measurements of the vapour–liquid coexistence densities and surface tensions of fully flexible Lennard–Jones chains ranging in length from 4 to 60 beads. We collapse the data according to Equation (1), and demonstrate that a universal behaviour is also observed for long polymer-like chains. The power-law scaling of the universal curve appears to be consistent with the theory of critical phenomena near the critical point, with a small deviation observed for longer chains at lower temperatures.

2. Computational methods

The model studied consists of fully flexible linear chains comprising M bonded beads. Non-bonded beads interacted through the Lennard-Jones potential,

$$U_{LJ}(r) = 4\varepsilon\left[\left(\frac{\sigma}{r}\right)^{12} - \left(\frac{\sigma}{r}\right)^{6}\right],$$

where r is the distance between two beads, ε is the energy well depth and σ sets the interaction range. For computational efficiency, the pair force computed from the gradient of U_{LJ} was truncated to zero at a cut-off distance $r_c = 6\sigma$ so that non-bonded forces acted only between pairs of particles with $r < r_c$. This cut-off distance has been shown to be sufficiently large to yield accurate coexistence densities for the simple Lennard–Jones fluid [23] and Lennard–Jones chain dimers [24]. Bonded beads interacted through a harmonic potential:

$$U_B(r) = \frac{k}{2}(r-\sigma)^2.$$

A stiff spring constant $k = 75,000\,\varepsilon/\sigma^2$ was employed in order to facilitate comparison of data with previous Monte Carlo simulations [17,18], where bond lengths are typically constrained to be exactly σ. The chosen value of k corresponds approximately to the value suggested for substituting harmonic bonds for constrained bonds in the TraPPE force field [25–28]. Molecular dynamics simulations were performed with the HOOMD-blue simulation package on general-purpose graphics processing units [29]. The equations of motion were integrated using the velocity-Verlet algorithm with time step $0.001\,\tau$, where $\tau = \sqrt{m\sigma^2/\varepsilon}$ is the derived unit of time and m is the mass of a bead. Isothermal conditions were maintained using a weakly coupled Langevin thermostat with friction factor $0.1\,m/\tau$ [30].

Chains of a given length ranging from $M = 4$ to $M = 60$ were initially placed randomly in a periodic cubic simulation box of edge length $L_x = L_y = L_z = 60\,\sigma$. We kept the total number of monomers roughly constant at 18, 750, and the number of chains varied from 4687 ($M = 4$) to 312 ($M = 60$). The simulation box was compressed at a constant rate for $5000\,\tau$ to an edge length $L_x = L_y = L_z = 30\,\sigma$, which gave a final density $\rho \approx 0.7\,\mathrm{m}/\sigma^3$. During compression, the temperature was held constant at $T = 4.0\,\varepsilon/k_B$, which is above the critical temperature for all chain lengths studied.

The simulation box was then expanded along the z-axis by a factor of 4 ($L_z = 120\,\sigma$) to yield a slab surrounded by vacuum. The fluid was quenched to a temperature below the critical point, and vapour–liquid equilibrium was established over a period of $15,000\,\tau$. For all chain lengths and temperatures, we observed that the liquid slab expanded to no more than roughly $L_z/2$, which we found to be sufficient to establish a bulk vapour phase. A representative snapshot of the final equilibrated state is shown in Figure 1 for $M = 20$ at $T = 2.7\,\varepsilon/k_B$. Production-quality simulation data were collected over $10,000\,\tau$ for five independent trajectories generated from statistically independent starting configurations and unique seeds to the Langevin thermostat pseudo-random number generator [31]. Statistical uncertainties were estimated based on the variance of quantities between the trajectories.

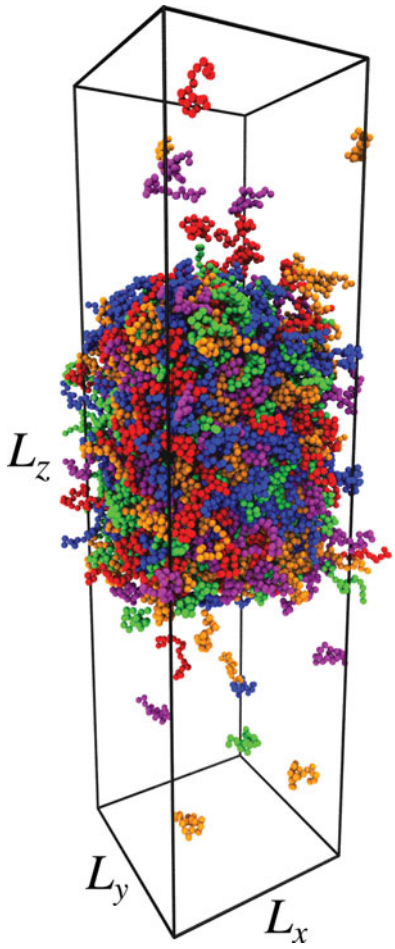

Figure 1. Visualisation [32] of vapour–liquid coexistence of $M = 20$ chains at $T = 2.7\,\varepsilon/k_B$.

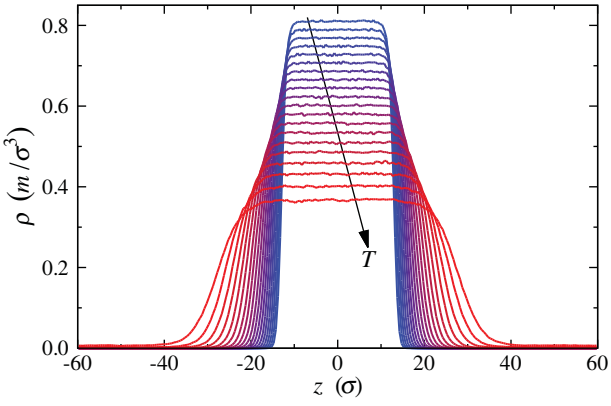

Figure 2. Density profiles $\rho(z)$ for chain length $M = 60$ from temperature $T = 1.4\,\varepsilon/k_B$ (top) to $T = 3.3\,\varepsilon/k_B$ (bottom).

Density profiles were computed along z from snapshots taken every $200\,\tau$ by dividing the simulation box into 240 bins of width $0.5\,\sigma$. Profiles were adjusted to remain centred at $z = 0$ to remove small drift of the liquid slab over long times and were subsequently averaged over the trajectories. A representative set of density profiles is shown in Figure 2 for chain length $M = 60$. The coexistence densities were computed by averaging the density in the bulk regions sufficiently far from the vapour–liquid interfaces.

The surface tension was calculated using the standard mechanical definition [33],

$$\gamma = \frac{L_z}{2}\left\langle P_{zz} - \frac{P_{xx} + P_{yy}}{2}\right\rangle,$$

where P_{xx}, P_{yy} and P_{zz} are the diagonal components of the pressure tensor along the x-, y- and z-axes, respectively, and the brackets denote an ensemble average. The factor of 1/2 accounts for the presence of two interfaces within the simulation box. Values of the pressure tensor were collected every $0.05\,\tau$ and averaged over the trajectories. The surface tension was corrected for truncation of the Lennard–Jones potential using the scheme proposed by Chapela *et al.* [34], which has been shown to be reliable for the chosen r_c [35]. Following this scheme, the average density profile was fit to a hyperbolic tangent form:

$$\rho(z) = \frac{\rho_L + \rho_V}{2} - \frac{\Delta\rho}{2}\tanh\left(\frac{z - z_0}{d}\right),$$

where z_0 is the position of the interface and d sets the interfacial thickness. (We note that the coexistence densities obtained by this fitting procedure are in complete agreement with the values obtained by averaging in the bulk.) The fitted values for d are reported in Tables 1–3. For a given chain length, d increases with temperature, as expected from Figure 2. The surface tension was corrected by $\Delta\gamma$ [34], where

$$\Delta\gamma = 12\pi\,(\Delta\rho)^2 \int_0^1 \mathrm{d}s \int_{r_c}^{\infty} \mathrm{d}r\,(r^{-3} - 2r^{-9}) \times (3s^3 - s)\coth\left(\frac{sr}{d}\right).$$

3. Results and discussion

3.1. Coexistence properties

The computed vapour–liquid phase diagrams, plotted in Figure 3 and tabulated in Tables 1–3, show behaviour characteristic of long chain molecules. The phase envelopes become wider and taller with respect to density and temperature, respectively, and skew to lower densities as chain length increases. The coexistence densities are in generally good agreement with values reported in the literature for a comparable cut-off radius [20] or with inhomogeneous long-ranged corrections to the Lennard–Jones potential [18]. In particular, we found agreement of the liquid density for $M = 8$ within 2% up to $T = 2.2\,\varepsilon/k_B$, with a 7% smaller liquid density at

Table 1. Coexistence densities, interfacial thicknesses and surface tensions for 4-, 6-, 8- and 10-bead chains. Subscript indicates uncertainty in the last reported digit.

$T\,(\varepsilon/k_B)$	$\rho_L\,(m/\sigma^3)$	$\rho_V\,(m/\sigma^3)$	$d\,(\sigma)$	$\gamma\,(\varepsilon/\sigma^2)$
		$M = 4$ (4687 chains)		
1.2	0.801_0	0.00018_2	1.10_0	0.99_1
1.3	0.774_0	0.00058_{11}	1.22_1	0.87_1
1.4	0.745_0	0.00142_7	1.37_2	0.75_1
1.5	0.716_0	0.0031_2	1.54_2	0.64_1
1.6	0.685_1	0.0062_1	1.72_2	0.53_1
1.7	0.652_0	0.0113_3	1.99_3	0.43_2
1.8	0.616_0	0.0199_4	2.30_4	0.31_2
1.9	0.576_0	0.0326_7	2.79_6	0.24_1
2.0	0.525_1	0.053_1	3.50_6	0.14_1
2.1	0.442_2	0.090_2	5.32_9	0.06_1
		$M = 6$ (3125 chains)		
1.4	0.770_0	0.00010_2	1.24_1	0.87_2
1.5	0.744_0	0.00035_4	1.38_1	0.77_3
1.6	0.718_0	0.00097_6	1.49_2	0.68_2
1.7	0.691_0	0.0020_1	1.66_2	0.57_2
1.8	0.662_1	0.0041_2	1.86_3	0.49_3
1.9	0.632_1	0.0073_1	2.11_4	0.40_2
2.0	0.600_1	0.0134_6	2.41_6	0.32_2
2.1	0.563_1	0.0220_7	2.82_4	0.23_1
2.2	0.521_0	0.0355_6	3.42_{14}	0.13_2
2.3	0.469_1	0.059_1	4.53_{11}	0.10_4
		$M = 8$ (2343 chains)		
1.6	0.733_0	0.00016_4	1.41_2	0.76_1
1.7	0.708_0	0.00039_8	1.54_2	0.64_2
1.8	0.683_0	0.0010_1	1.69_3	0.55_3
1.9	0.656_1	0.0022_2	1.88_2	0.46_2
2.0	0.627_1	0.0042_1	2.13_3	0.41_4
2.1	0.597_1	0.0076_3	2.34_4	0.33_2
2.2	0.565_0	0.0139_8	2.72_7	0.27_2
2.3	0.529_0	0.0227_4	3.24_8	0.18_1
2.4	0.487_1	0.0364_4	3.88_{10}	0.12_3
2.5	0.430_2	0.062_3	5.58_{16}	0.09_4
		$M = 10$ (1875 chains)		
1.7	0.718_1	0.00007_3	1.47_1	0.69_2
1.8	0.693_0	0.0002_1	1.61_2	0.63_1
1.9	0.669_0	0.0007_2	1.77_2	0.55_2
2.0	0.643_1	0.0016_2	1.94_3	0.45_2
2.1	0.615_0	0.0033_4	2.16_4	0.37_2
2.2	0.587_1	0.0062_4	2.41_5	0.32_4
2.3	0.556_1	0.0102_3	2.79_6	0.25_2
2.4	0.522_1	0.0170_6	3.20_6	0.17_1
2.5	0.483_2	0.029_1	3.93_9	0.12_3
2.6	0.434_1	0.051_3	5.13_{17}	0.06_2

$T = 2.5\,\varepsilon/k_B$. Given that substitution of harmonic bonds with $k = 3000\,\epsilon/\sigma^2$ for rigid bonds in [20] had only a negligible effect on the coexistence densities compared to [18] and that all works give very good agreement at temperatures far below the critical point, we attribute this discrepancy to finite-size scaling effects near the critical point [36]. The simulation box in this work has a cross-sectional edge length ($L_x = L_y = 30\,\sigma$) roughly three times larger than in [18,20] ($L_x = L_y = 11\,\sigma$), and so the values reported here should more accurately reflect the infinite-size limit.

Critical points were estimated by extrapolation using the law of rectilinear diameters:

$$\frac{\rho_L + \rho_V}{2} = \rho_c + A(T_c - T),$$

Table 2. Coexistence densities, interfacial thicknesses and surface tensions for 20-, 30- and 40-bead chains. Subscript indicates uncertainty in the last reported digit.

$T\,(\varepsilon/k_B)$	$\rho_L\,(m/\sigma^3)$	$\rho_V\,(m/\sigma^3)$	$d\,(\sigma)$	$\gamma\,(\varepsilon/\sigma^2)$
		$M = 20$ (937 chains)		
2.0	0.670_1		1.68_2	0.59_2
2.1	0.647_0	0.00004_3	1.83_3	0.51_2
2.2	0.624_1	0.00011_5	2.01_4	0.46_3
2.3	0.599_1	0.0004_2	2.21_2	0.40_2
2.4	0.575_1	0.0009_2	2.43_3	0.33_3
2.5	0.549_1	0.0024_4	2.69_6	0.25_4
2.6	0.519_1	0.0043_4	2.95_8	0.26_3
2.7	0.490_1	0.0080_6	3.40_8	0.19_3
2.8	0.456_1	0.0138_9	4.05_7	0.12_3
2.9	0.419_1	0.025_1	4.92_{18}	0.10_2
		$M = 30$ (625 chains)		
2.1	0.657_0		1.75_2	0.55_2
2.2	0.634_1		1.88_3	0.45_4
2.3	0.612_0		2.04_3	0.45_2
2.4	0.589_1		2.21_3	0.39_3
2.5	0.565_1	0.0003_1	2.43_3	0.32_2
2.6	0.540_1	0.0005_2	2.64_4	0.28_2
2.7	0.514_1	0.0014_5	2.97_8	0.23_4
2.8	0.486_1	0.0026_4	3.30_7	0.18_3
2.9	0.456_1	0.006_1	3.80_{10}	0.13_3
3.0	0.422_1	0.011_1	4.56_{24}	0.11_3
		$M = 40$ (468 chains)		
2.2	0.640_1		1.87_2	0.53_2
2.3	0.618_1		1.99_3	0.46_2
2.4	0.595_1		2.16_5	0.42_2
2.5	0.573_1		2.31_2	0.34_3
2.6	0.549_0	0.00010_9	2.48_2	0.29_3
2.7	0.523_1	0.0002_2	2.75_6	0.27_1
2.8	0.498_0	0.0007_4	3.04_{12}	0.20_5
2.9	0.471_0	0.0019_4	3.41_6	0.17_3
3.0	0.443_1	0.0034_5	3.92_8	0.17_2
3.1	0.410_1	0.0080_7	4.50_{15}	0.10_3

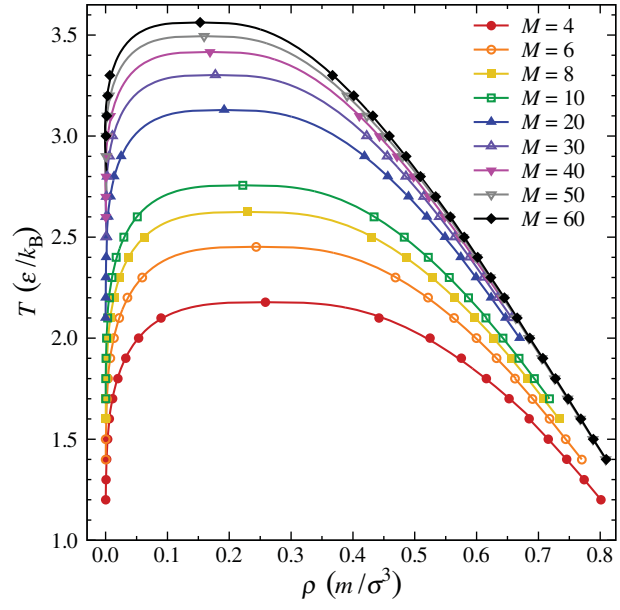

Figure 3. Vapour–liquid coexistence densities for chain lengths from $M = 4$ to $M = 60$. Solid lines show the extrapolation to the critical point for the top six data points, and are a guide to the eye otherwise. Statistical uncertainty is smaller than symbol size.

Table 3. Coexistence densities, interfacial thicknesses, and surface tensions for 50- and 60-bead chains. Subscript indicates uncertainty in the last reported digit.

$T\,(\varepsilon/k_B)$	$\rho_L\,(m/\sigma^3)$	$\rho_V\,(m/\sigma^3)$	$d\,(\sigma)$	$\gamma\,(\varepsilon/\sigma^2)$
		$M = 50$ (375 chains)		
1.4	0.809_0		1.07_1	1.11_2
1.5	0.788_0		1.14_1	1.01_1
1.6	0.767_1		1.23_1	0.91_2
1.7	0.747_0		1.31_1	0.87_1
1.8	0.726_0		1.40_2	0.78_2
1.9	0.706_0		1.48_1	0.73_1
2.0	0.685_0		1.60_2	0.64_1
2.1	0.664_0		1.71_2	0.61_3
2.2	0.643_0		1.84_3	0.54_4
2.3	0.621_1		1.97_3	0.47_1
2.4	0.600_0		2.10_4	0.39_2
2.5	0.577_0		2.25_3	0.39_1
2.6	0.555_1		2.50_6	0.33_3
2.7	0.531_1		2.65_3	0.28_2
2.8	0.507_1		2.92_8	0.23_4
2.9	0.480_1	0.0008_4	3.26_6	0.20_3
3.0	0.452_2	0.0012_6	3.61_6	0.16_2
3.1	0.423_1	0.0027_8	4.22_{13}	0.12_3
3.2	0.391_2	0.0057_8	4.81_6	0.11_3
		$M = 60$ (312 chains)		
1.4	0.810_0		1.06_2	1.11_2
1.5	0.789_0		1.13_1	1.01_3
1.6	0.769_0		1.20_2	0.96_2
1.7	0.748_0		1.29_2	0.87_2
1.8	0.728_0		1.38_3	0.79_4
1.9	0.707_0		1.48_2	0.74_2
2.0	0.686_1		1.60_3	0.66_2
2.1	0.666_0		1.67_3	0.60_4
2.2	0.645_0		1.80_3	0.52_3
2.3	0.623_1		1.92_2	0.52_4
2.4	0.602_0		2.07_3	0.41_0
2.5	0.580_1		2.24_3	0.37_5
2.6	0.558_1		2.39_3	0.35_2
2.7	0.534_1		2.63_6	0.28_6
2.8	0.509_1		2.79_7	0.25_2
2.9	0.486_1		3.10_8	0.21_1
3.0	0.459_1	0.0007_6	3.43_5	0.20_3
3.1	0.432_1	0.0018_{12}	3.95_{10}	0.18_5
3.2	0.401_1	0.0032_9	4.57_{12}	0.11_3
3.3	0.367_2	0.0068_6	5.27_{22}	0.07_5

in conjunction with the universal scaling of the coexistence densities near the critical point

$$\Delta\rho = \Delta\rho_0(1 - T/T_c)^{\beta}, \tag{2}$$

where A and $\Delta\rho_0$ are material-specific fitting parameters. We assume $\beta \approx 0.325$ based on the three-dimensional Ising model universality class [37]. The extrapolation was performed using data from the six highest temperatures for each chain length because Equation (2) is only valid asymptotically close to the critical point. Using fewer points did not significantly change the estimate of the critical point (less than 1%). Statistical uncertainty for the critical points was estimated synthetically from the uncertainties in the coexistence densities. The reported uncertainties do not account for systematic errors inherent to the method of estimation. The extrapolated critical points are reported in Figure 3 and Table 4.

Table 4. Tabulated critical points. Subscript indicates uncertainty in the last reported digit.

M	$T_c\,(\varepsilon/k_B)$	$\rho_c\,(m/\sigma^3)$
4	2.18_0	0.259_2
6	2.45_0	0.244_1
8	2.62_1	0.230_2
10	2.76_1	0.222_2
20	3.13_0	0.192_2
30	3.30_1	0.178_1
40	3.42_1	0.169_1
50	3.49_1	0.159_2
60	3.56_1	0.153_2
∞	4.34	0

Qualitatively, the critical temperature increases to approach an asymptotic value with increasing molecular weight, while the critical density decreases towards zero. We extrapolated the critical temperature to infinite molecular weight, T_c^{∞}, according to the Shultz–Flory relationship [38]:

$$1/T_c - 1/T_c^{\infty} \sim 1/\sqrt{M} + 1/2M,$$

and determined $T_c^{\infty} \approx 4.34\,\varepsilon/k_B$. The Shultz–Flory plot linearised the data remarkably well over the entire range of M investigated. We found that ρ_c decays to zero as a power law, $\rho_c \sim M^{-0.20}$, for all but the shortest chain length. This scaling is consistent with that observed by Sheng *et al.* for a similar Lennard–Jones chain polymer model [21], but more slowly decaying than the Flory–Huggins prediction, $\rho_c \sim 1/\sqrt{M}$.

In principle, the coexistence pressure can also be measured from $\langle P_{zz}\rangle$. This pressure is small for most temperatures considered due to the low density of chains in the vapour phase, and the relative uncertainty of the measurement is large. Accordingly, we have chosen not to report the directly measured coexistence pressure. Instead, the coexistence pressure can be conveniently estimated from the ideal gas law, $P \approx (\rho_V/Mm)k_BT$, in this low-density limit.

3.2. Surface tension

The surface tension is shown as a function of temperature for different chain length in Figure 4 and in Tables 1–3. As expected, the surface tension decreases with temperature for a fixed chain length, and increases with chain length for a fixed temperature. The surface tension should decrease to zero as temperature approaches the critical point according to

$$\gamma = \gamma_0(1 - T/T_c)^{\mu}, \tag{3}$$

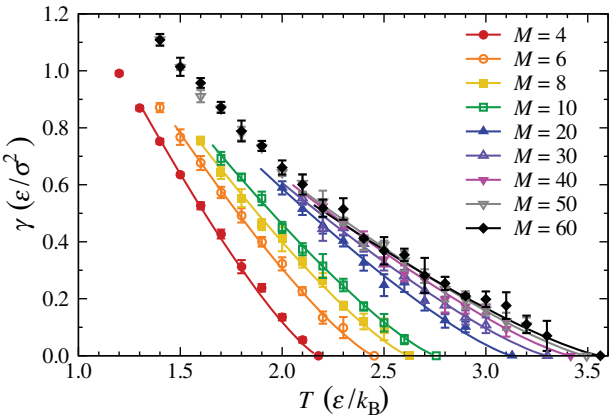

Figure 4. Surface tension for chain lengths from $M = 4$ to $M = 60$. Simulation data are given by points, while fits to eq. (3) are shown by lines. Fits are obtained using $T \geq 0.6\ T_c$.

where γ_0 is a material-specific fitting parameter, and we have assumed $\mu \approx 1.26$ based on Widom's hyperscaling relationship for the three-dimensional Ising model universality class [37,39]. As with Equation (2), Equation (3) is strictly only valid near the critical point. We fit the surface tension to Equation (3) for $T \geq 0.6\ T_c$, and the resulting curves are shown in Figure 4. Equation (3) appears to fit the data well across all temperatures for $M \leq 40$. We observed a deviation from Equation (3) for the 50- and 60-bead chains at temperatures below $0.6\ T_c$.

We reduced the surface tension according to eq. (1), shown in Figure 5. The data appear to collapse onto a universal curve for all chain lengths and temperatures measured. Our data extend the range of $\Delta\rho/\rho_c$ by a factor of two compared to what has previously been investigated [15]. We attempted to fit the collapsed data to eq. (1) in order to extract a value for p, but found that the data was not well-described by a single exponent for all $\Delta\rho/\rho_c$ measured. We performed a nonlinear least-squares fit of

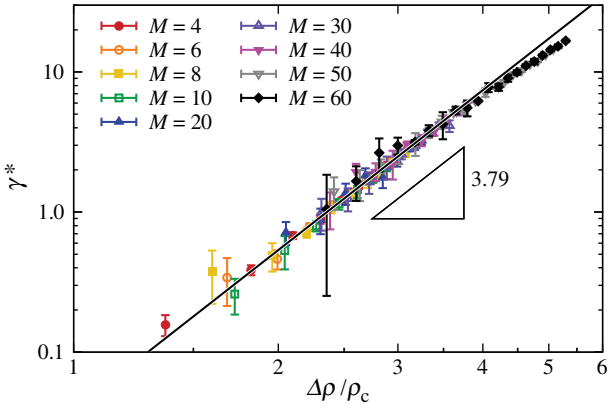

Figure 5. Reduced surface tension as a function of reduced density difference for chain lengths from $M = 4$ to $M = 60$. The fitted power-law exponent is 3.79 ± 0.05.

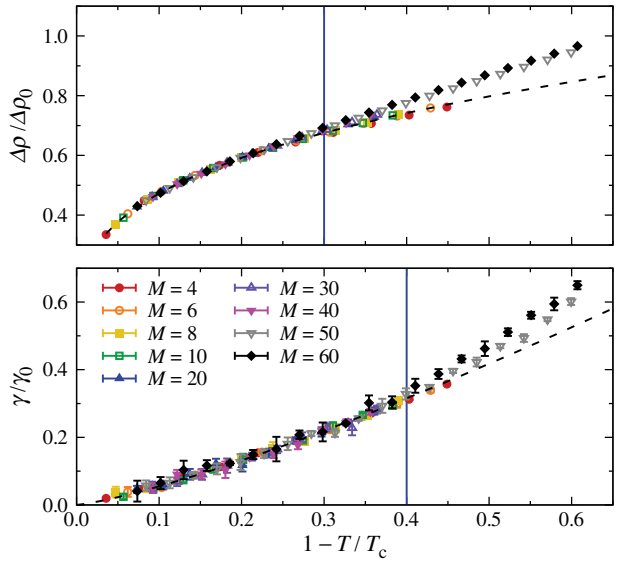

Figure 6. Reduced coexistence density difference $\Delta\rho/\Delta\rho_0$ (top) and reduced surface tension γ/γ_0 (bottom) as a function of reduced temperature. Vertical line indicates estimated point of deviation from critical scaling laws for $M = 50$ and $M = 60$ chains. Statistical uncertainty due to sampling is smaller than symbol size for $\Delta\rho/\Delta\rho_0$.

the data, weighted by the sampling uncertainty, for $\Delta\rho/\rho_c < 3$ and found $p = 3.79 \pm 0.05$. This fitted value for p deviates slightly from the value of 3.55 reported by Galliero for Mie n-6 fluids over a comparable range of $\Delta\rho/\rho_c$ [12]; this 6% discrepancy may simply be due to the method of fitting or uncertainty in the measurements.

Close to the critical point, eqs. (2) and (3) require that $p = 3.87$. The fitted value of p is reasonably consistent with this prediction (2% error). We plotted $\Delta\rho/\Delta\rho_0$ and γ/γ_0 against the reduced temperature in Figure 6. Such a plot should yield a universal curve in the regimes where eqs. (2) and (3) are valid. We confirmed that $\Delta\rho$ and γ show universal scaling near the critical point, with the first deviation observed for $\Delta\rho$ at roughly $T \approx 0.7\ T_c$. To ensure we fitted to data close the critical point, we refit for $T \geq 0.8\ T_c$, and found $p = 3.83 \pm 0.07$. This would suggest that $p = 3.87$ can be obtained asymptotically close to the critical point, but in practice a lower effective exponent is observed because (1) measurement temperatures are farther from the critical point, and (2) the fitted exponent is sensitive to uncertainty in the collapsed data.

The reduced surface tension appears to deviate most significantly from the power-law fit for the 50- and 60-bead chains when $\Delta\rho/\rho_c > 4$. These points correspond to $T < 0.7\ T_c$ for the 50- and 60-bead chains, which is consistent with Figure 6. We refit the data in this region to Equation (1) found $p = 3.13 \pm 0.05$. The reason for this change in exponent is not obvious. One might speculate that there is a possible cross-over to the mean field

theory prediction $p = 3$ [37] for conditions far from the critical point, but there are insufficient measurements in this range of $\Delta\rho/\rho_c$ to assess this. Given that the relevant processing temperatures for many high-molecular-weight polymers is far below the critical temperature, this deviation warrants further investigation.

4. Conclusions

We determined the vapour–liquid coexistence densities and surface tension of fully flexible Lennard–Jones chains up to 60 beads in length using molecular dynamics simulations. We showed that the universal parachor correlation reduces the data to a single master curve for all chain lengths. We fit a universal parachor exponent $p = 3.79 \pm 0.05$ for conditions close to the critical point, which is reasonably consistent with the predictions of the theory of universal critical phenomena. A smaller parachor exponent was observed for longer chains far from the critical point. In order to assess the significance of this deviation, data are needed for longer chains at temperatures far below the critical point in order to extend the range of $\Delta\rho/\rho_c$ measured. However, simulating over the polymer relaxation times necessary to establish vapour–liquid equilibrium and reliably measure the surface tension present a considerable computational challenge. These measurements are left as a possible subject for future work.

Disclosure statement

No potential conflict of interest was reported by the authors.

Funding

The financial support for this work was provided by the Princeton Center for Complex Materials (PCCM), a U.S. National Science Foundation Materials Research Science and Engineering Center [grant number DMR-1420541]. M.P. Howard received Government support under contract FA9550-11-C-0028 and awarded by the Department of Defense, Air Force Office of Scientific Research, National Defense Science and Engineering Graduate (NDSEG) Fellowship, 32 CFR 168a.

ORCID

Kevin S. Silmore http://orcid.org/0000-0001-8464-8100
Michael P. Howard http://orcid.org/0000-0002-9561-4165
Athanassios Z. Panagiotopoulos http://orcid.org/0000-0002-8152-6615

References

[1] M. Nobakht, S. Moghadam, and Y. Gu, Energy Fuels **21**(6), 3469–3476 (2007).
[2] S.R. Forrest and M.E. Thompson, Chem. Rev. **107**(4), 923–925 (2007).
[3] G.T. Dee and B.B. Sauer, Adv. Phys. **47**(2), 161–205 (1998).
[4] P.J. Linstrom and W.G. Mallard, editors,*NIST Chemistry WebBook, NIST Standard Reference Database Number 69* (National Institute of Standards and Technology, Gaithersburg, MD, 2015).
[5] J.J. Jasper, J. Phys. Chem. Ref. Data **1**(4), 841–1010 (1972).
[6] S. Wu, J. Macromol. Sci., Rev. Macromol. Chem. **10**(1), 1–73 (1974).
[7] J.M. Garrido, A. Mejía, M.M. Piñeiro, F.J. Blas and E.A. Müller, AIChE J. **62**(5), 1781–1794 (2016).
[8] D.B. Macleod, Trans. Faraday Soc. **19**, 38–41 (1923).
[9] S. Sugden, J. Chem. Soc., Trans. **125**, 1177–1189 (1924).
[10] E.A. Guggenheim, J. Chem. Phys. **13**(7), 253 (1945).
[11] D. Broseta, Y. Meleán, and C. Miqueu, Fluid Phase Equilib. **233**(1), 86–95 (2005).
[12] G. Galliero, M.M. Piñeiro, B. Mendiboure, C. Miqueu, T. Lafitte, and D. Bessieres, J. Chem. Phys. **130**(10), 104704 (2009).
[13] G. Galliero, J. Chem. Phys. **133**(7), 074705 (2010).
[14] J.K. Johnson, E.A. Müller, and K.E. Gubbins, J. Phys. Chem. **98**(25), 6413–6419 (1994).
[15] F.J. Blas, F.J. Martínez-Ruiz, A.I.M.V. Bravo, and L.G. MacDowell, J. Chem. Phys. **137**(2), 024702 (2012).
[16] D. Duque, J.C. Pàmies, and L.F. Vega, J. Chem. Phys. **121**(22), 11395 (2004).
[17] F.J. Blas, L.G. MacDowell, E. de Miguel, and G. Jackson, J. Chem. Phys. **129**(14), 144703 (2008).
[18] L.G. MacDowell and F.J. Blas, J. Chem. Phys. **131**(7), 074705 (2009).
[19] F.J. Blas, A.I.M.V. Bravo, J. Algaba, F.J. Martínez-Ruiz, and L.G. MacDowell, J. Chem. Phys. **140**(11), 114705 (2014).
[20] P.V. Ramírez-González, S.E. Quiñones-Cisneros, and U.K. Deiters, Mol. Phys. **113**(1), 28–35 (2014).
[21] Y.J. Sheng, A.Z. Panagiotopoulos, S.K. Kumar, and I. Szleifer, Macromolecules **27**(2), 400–406 (1994).
[22] F.A. Escobedo and J.J. dePablo, Mol. Phys. **87**(2), 347–366 (1996).
[23] A. Trokhymchuk and J. Alejandre, J. Chem. Phys. **111**(18), 8510–8523 (1999).
[24] D. Duque and L.F. Vega, J. Chem. Phys. **121**(17), 8611 (2004).
[25] C.J. Mundy, J.I. Siepmann, and M.L. Klein, J. Chem. Phys. **102**(8), 3376–3380 (1995).
[26] M.G. Martin and J.I. Siepmann, J. Phys. Chem. B **102**(14), 2569–2577 (1998).
[27] J.P. Nicolas and B. Smit, Mol. Phys. **100**(15), 2471–2475 (2009).
[28] J.C. Pàmies, C. McCabe, P.T. Cummings, and L.F. Vega, Mol. Simul. **29**(6-7), 463–470 (2010).
[29] J.A. Anderson, C.D. Lorenz, and A. Travesset, J. Comput. Phys. **227** (10), 5342–5359 (2008); J. Glaser, T.D. Nguyen, J.A. Anderson, P. Lui, F. Spiga, J.A. Millan, D.C. Morse, and S.C. Glotzer, Comput. Phys. Commun. **192**, 97–107 (2015).
[30] M.P. Allen and D.J. Tildesley, *Computer Simulation of Liquids* (Oxford University Press, New York, 1991).
[31] C.L. Phillips, J.A. Anderson, and S.C. Glotzer, J. Comput. Phys. **230**(19), 7191–7201 (2011).

[32] W. Humphrey, A. Dalke and K. Schulten, J. Molec. Graphics **14**, 33–38 (1996).
[33] J.G. Kirkwood and F.P. Buff, J. Chem. Phys. **17**(3), 338–343 (1949).
[34] G.A. Chapela, G. Saville, S.M. Thompson, and J.S. Rowlinson, J. Chem. Soc., Faraday Trans. 2 **73**, 1133–1144 (1977); J. Alejandre, D.J. Tildesley and G.A. Chapela, Mol. Phys. **85** (3), 651–663 (1995); E.M. Blokhuis, D. Bedeaux, C.D. Holcomb, and J.A. Zollweg, Mol. Phys. **85**(3), 665–669 (1995).
[35] F. Goujon, A. Ghoufi, P. Malfreyt and D.J. Tildesley, J. Chem. Theory Comput. **11**(10), 4573–4585 (2015).
[36] D.P. Landau and K. Binder, *A Guide to Monte-Carlo Simulations in Statistical Physics*, 3rded. (Cambridge University Press, Cambridge, 2009).
[37] J.S. Rowlinson and B. Widom, *Molecular Theory of Capillarity* (Dover Publications, Mineola, NY, 2002).
[38] A.R. Shultz and P.J. Flory, J. Am. Chem. Soc. **74**(19), 4760–4767 (1952).
[39] B. Widom, J. Chem. Phys. **43**(11), 3892 (1965).